Rebound effects caused by withdrawal of MET kinase inhibitor are quenched by a MET therapeutic antibody

Emanuela Pupo[1], Nadia Ducano[1], Barbara Lupo[2,5], Elisa Vigna[3,5], Daniele Avanzato[1],

Timothy Perera[6], Livio Trusolino[2,5], Letizia Lanzetti[1,5*] and Paolo M. Comoglio[4,5*].

[1]Membrane Trafficking, [2]Translational Cancer Medicine, [3]Gene Transfer and Therapy, [4]Molecular Therapeutics and Exploratory Research Laboratories at Candiolo Cancer Institute – FPO, IRCCS, Str. Provinciale 142, 10060 Candiolo, Italy

[5]Department of Oncology, University of Torino Medical School

[6]Octimet Oncology Ltd, OX44 7UE Oxfordshire, UK.

*These authors equally contributed to the work

Running title: "Removal of MET kinase inhibition causes tumor rebound"

Keywords: MET, rebound, endocytosis, oncogene addiction, ATP-competitive inhibitors

Correspondence should be addressed to:

Letizia Lanzetti
FPO, IRCCS
Str. Provinciale 142, 10060 Candiolo,
Turin Italy
Tel. +39 0119933255
Fax +39 0119933524
e-mail: letizia.lanzetti@ircc.it

Paolo M. Comoglio
FPO, IRCCS
Str. Provinciale 142, 10060 Candiolo,
Turin Italy
Tel. +39 0119933601
Fax +39 0119621525
e-mail: paolo.comoglio@ircc.it

Conflict of interest

E. Pupo, N. Ducano, B. Lupo, D. Avanzato, L. Trusolino, E. Vigna and L. Lanzetti declare no conflict of interest. P. Comoglio has recently been consultant for Metheresis. T. Perera is a founder of OCTIMET Oncology Ltd, UK.

Word count 5304

Number of Figures 7

ABSTRACT

MET oncogene amplification is emerging as a major mechanism of acquired resistance to EGFR-directed therapy in lung and colorectal cancers. Further, MET amplification predicts responsiveness to MET inhibitors currently in clinical trials. Among the anti-MET drugs available, ATP-competitive small molecule kinase inhibitors abrogate receptor autophosphorylation and downstream activation of ERK1/2 and AKT, resulting in cell cycle arrest. However, this anti-proliferative effect allows persistence of a pool of cancer cells that are quiescent but alive. Once the inhibition is removed, rebound activation of MET-driven cell proliferative pathways and tumor growth may occur, an adverse event observed frequently in clinical settings after drug discontinuation. Here we show that inhibitor withdrawal prompts receptor phosphorylation to levels higher than those displayed at steady-state and generates a rebound effect pushing quiescent cancer cells back into the cell cycle, both in vitro and in experimental tumor models in vivo. Mechanistically, we found that inhibitor treatment blocks MET endocytosis, causing a local increase in the number of receptors at the plasma membrane. Upon inhibitor washout, the receptor is readily re-phosphorylated. The initial phosphorylation is not only increased but also prolonged in duration due to downmodulation of a phosphatase-mediated MET negative feedback loop which accompanies receptor internalization. Notably, treatment with a MET therapeutic antibody that induces proteolytic cleavage of the receptor at the cell surface substantially prevents this rebound effect, providing a rationale to combine or alternate these mechanistically different types of MET-targeted therapy.

INTRODUCTION

Receptor tyrosine kinases (RTKs) are major targets for pharmaceutical inhibition due to their crucial role in oncogenesis and progression of many solid tumors. Several small molecular weight inhibitors have been developed that, by inhibiting tyrosine kinase activity of oncogenic RTKs, abrogate their downstream signaling cascade and impair cancer cell proliferation (1).

The rationale of targeting the MET kinase stems from the observation that this receptor is aberrantly activated in tumors. Upregulation is achieved by gene amplification, enhanced transcription or ligand-dependent autocrine loops (2,3). Moreover, activating somatic mutations have also been reported (2,4). Tumors carrying *MET* amplification are dependent on MET signaling for growth and survival, as inhibition of MET in *MET*-amplified cancer cells severely impairs cell proliferation, a phenomenon termed 'oncogene addiction' (5). In 'addicted cells', MET kinase inhibition abrogates downstream ERK1/2 and AKT phosphorylation, resulting in cell cycle arrest. However, even under conditions of prolonged pharmacological MET inhibition, a pool of cells remains quiescent without being irreversibly committed to apoptosis and resume growth after release of MET blockade (6). Although the molecular mechanisms of tyrosine kinase inhibitors have been extensively studied, the effects of drug withdrawal on cancer cells are still largely unexplored.

Here we investigated the effects of removal of a MET kinase inhibitor both *in vitro* and in experimental tumor models *in vivo*.

4

MATERIALS AND METHODS

Cell culture

A549, H1993 and EBC-1 cells were grown in RPMI, Hs746T in Iscove's Dulbecco modified medium (Sigma) supplemented with 10% FBS (Euroclone) and 1% glutamine. A549, H1993 and Hs746T cells were obtained from the European Collection of Cell Cultures, EBC-1 cells were from the Japanese Collection of Research Bioresources.

The genetic identity of the cell lines was confirmed by short tandem repeat profiling (Cell ID, Promega), which was last repeated in November 2015. Cells were periodically tested and resulted negative for mycoplasma contamination with Venor GM kit (Minerva biolabs).

Immunofluorescence and quantifications

In the endocytosis assays, cells were plated on 24 well plates (50.000 cells/well for A549 and H1993, 70.000 cells/well for Hs746T). The day after, cells were starved in serum free medium supplemented with 0.2% BSA for 4 hours at 37°C then incubated for 1 hour at 4°C in presence of HGF [50 ng/ml] or of purified anti-MET (DO24) or control unrelated antibodies [85.7 µg/ml]. JNJ-605 300nM was added or not during this incubation step and left throughout the following internalization step. Cells were then shifted at 37°C for 15 min to allow MET endocytosis. Immunofluorescence was as in (7) staining cells with anti-MET (DO24) and anti-EEA1 antibodies. Primary antibodies were revealed by Alexa Fluor 555-, 488- (Molecular Probes, USA) conjugated secondary antibodies. Confocal analysis was performed on a Leica TCS SP5 AOBS microscope and processed in Adobe Photoshop. Immunofluorescence acquisition settings were kept constant within each cell line. Quantitative analyses of co-localization were carried out with ImageJ software (http://rsb.info.nih.gov/ij/) using the JacoP plugin (Manders coefficient). The phospho-MET

and total MET ratio was calculated with ImageJ measuring the mean pixel intensity in each channel, background subtracted.

Endocytosis and Recycling biochemical assays

Endocytosis and Recycling assays were performed following the protocol described in (8,9). Briefly, cells were labeled at 4°C with 0.5 mg/ml sulfo-NHS-SS-biotin (ThermoScientific) in PBS for 30 min in presence or absence of 500nM JNJ-605. After washing, cells were transferred to pre-warmed medium and incubated at 37 °C for 15 min to allow endocytosis of biotinylated receptors in presence or absence of 500nM JNJ-605. In A549 cells, MET endocytosis was stimulated by treatment with HGF (50 ng/ml). Biotinylated MET was captured by overnight incubation of 50 µl cell lysate at 4°C using 96 multi-well immuno-plate (Sigma M5785-1Cs) coated with 5 µg/ml anti-MET DO24 antibody and revealed by ELISA with streptavidin-conjugated horseradish peroxidase (Amersham) followed by a chromogenic reaction with ortho-phenylenediamine (Sigma).

Measurement of surface MET

Cells were plated on 10 cm dishes (A549 and Hs746T 1.5 x 10^6 cells/well, EBC-1 2 x 10^6 cells/well) and treated, the day after, with JNJ-605 500nM for 2, 10 or 24 hours.

Cells were rinsed three times with cold PBS and surface receptors were biotinylated for 30 min at 4°C using the ECL protein biotinylation kit (GE Healthcare) according to the manufacturer's instructions. Cells were lysed in EB buffer: [20 mM Tris HCl pH 7.4, 2 mM EGTA, 5 mM EDTA, 150 mM NaCl, 10% glycerol, 1% Triton X-100, 50 mM Hepes]. Total cellular lysates were cleared by centrifugation and MET was immunoprecipitated from 300 µg of A549, 25 µg of EBC-1 and 50 µg of Hs746T of lysates with the anti-MET DQ13

antibody. Samples were run on SDS PAGE and blotted with HRP-conjugated streptavidin (GE Healthcare) and with anti-MET antibody DL21.

Analysis of inhibitor withdrawal in immunofluorescence, western blot, Multiplex phosphoproteomic and Cytofluorimetric experiments

In the immunofluorescence experiments H1993 cells were plated on 24 well plates (50.000 cells/well). The day after, cells were treated or not with 500nM JNJ-605 for 17 hours and then released by washing three times with 1 ml of medium. Next cells were incubated at 37°C with fresh medium for 15 min, then the entire procedure was repeated. Cells were fixed at various time points and stained.

For western blotting, MesoScale and cytofluorimetric experiments H1993 and EBC-1 cells were plated (400.000 cells in 19.5 cm^2 plate), treated or not with JNJ-605 500nM for 17 hours. Cells were released by washing them 3 times with 4 ml of medium and re-incubated at 37°C with fresh medium. After 15 min the release procedure was repeated. Samples were processed after the release at different time points as indicated. When indicated, MvDN30 and control Fab unrelated antibodies (50 µg/ml) were added after the second washout and cells were harvested 24 hours later. Western blot samples were lysed in EB buffer.

For the multiplex phosphoproteomic analyses we used commercially available plates from MesoScale Discovery of phospho-ERK/total ERK and phospho-AKT/total AKT. After incubation with protein extracts, detection was performed by quantitative electrochemiluminescence with reported antibodies coupled with SULFO-TAG as described in (6). The percentage of phosphorylated protein was calculated with the following formula: % phosphoprotein = [(2xphospho-signal)/(phospho-signal + total-signal)] x100. The percentage obtained was control subtracted, converted in logarithmic form and represented with the heat maps generated by the freeware Gedas program (10).

Cytofluorimetric analysis was performed using the Click-iT® EdU Alexa Fluor® 647 Flow Cytometry Assay Kit (Life Technologies). Cells were incubated for 2 hours with 10nM EdU, a thymidine analogue that is incorporated into DNA during DNA synthesis. Next cells were washed once with PBS and once with PBS 1% BSA, fixed, permeabilized and stained following the manufacturer's protocol. Samples were acquired using the CyAn ADP (Beckman Coulter). For statistical analyses the non-parametric Mann-Whitney test was used.

In vivo **experiments**

All animal procedures were performed according to protocols approved by Ethical Committee for animal experimentation of the Fondazione Piemontese per la Ricerca sul Cancro and by Italian Ministry of Health. Mice (female non-obese diabetic/severe combined immunodeficient -NOD/SCID- mice) were purchased from Charles River Laboratories. EBC-1 cells, 1.8×10^6 cells/mouse were injected subcutaneously into the right posterior flank of 6-week-old NOD-SCID mice. Tumor growth was evaluated periodically with a caliper and tumor volume was calculated as described (11). After 19 days, when masses reached on average tumor volumes of 118.5 ± 56 mm^3 mice were randomized and divided in 4 groups: one group was untreated (CTR, *n*=5), while the other 2 groups were treated with JNJ-605 (50 mg/kg) by gavage every 24 hours for 5 days. Of these, one did not receive any further administration (w/o JNJ-605, *n*=6) while the other (w/o JNJ-605 w MvDN30PEG, *n*=5) was treated with MvDN30-PEG (12) (15 mg/kg) every three days (day 23, 26, 29). At day 29, mice were injected intra-peritoneally with 75 µg/mouse of EdU in 200 µl of PBS. Twenty-four hours later mice were sacrificed and tumor were extracted, formalin-fixed, embedded in paraffin and sectioned. Tumor slices (3 µm thickness) were processed to highlight cells having incorporated EdU. Briefly, paraffin removal was performed with two 10 minutes steps in Xylene, slices were then washed twice with BSA 3% in PBS for 5 minutes, permeabilized

in PBS, 0.1% TritonX-100 (20 minutes at RT) and stained using the Click-iT® EdU AlexaFluor® 555 Imaging Kit (Life Technologies), following the manufacturer's instructions and with DAPI.

Statistical analysis was performed with Graphpad software using the non-parametric Mann-Whitney test.

The sources and applications of antibodies, growth factors and chemicals are detailed in the Supplementary Materials and Methods along with methods for the endocytosis assays shown in Supplementary Fig. S1, the HGF labeling and the *in vivo* experiment of Supplementary Fig. S6.

RESULTS

Kinase inhibition blocks MET endocytosis, but not recycling from endosomal compartments

We initially looked at the effects of MET kinase inhibition on the intracellular distribution of the receptor in *MET*-amplified H1993 (non-small cell lung cancer) and Hs746T (gastric cancer) cells (13). At steady state, MET localized mainly at the plasma membrane and in EEA1-positive early endosomes (Fig. 1A,D). Treatment with the MET-specific ATP-competitor JNJ-605 for two hours at 37°C abruptly reduced the amount of MET in early endosomes (Fig. 1A-F), suggesting that kinase inhibition blocks MET internalization and/or its intracellular trafficking.

First, we investigated whether the inhibition of MET kinase activity interferes with receptor endocytosis, either constitutive or induced by the ligand Hepatocyte Growth Factor (HGF), or by the agonistic anti-MET antibody, DO24 (14). The percentage of MET co-localizing with EEA1 in early endosomes was evaluated as a measure of receptor endocytosis. In the A549 cell line, featuring a normal gene copy number and expressing physiological amounts of the receptor at the surface, stimulation with HGF or DO24 caused MET endocytosis in EEA1-positive endosomes (Fig. 2A, top row, and C). In untreated H1993 and Hs746T cells, the amount of MET in endosomes was higher compared to A549 cells (Fig. 2A, middle and bottom rows, and C) indicative of constitutive endocytosis which likely results from basal phosphorylation of MET in these cell lines (13,15,16). Inhibition of MET kinase activity by JNJ-605 prevented MET endocytosis triggered by any treatment or resulting from receptor overexpression (Fig. 2B,C and Supplementary Fig. S1A-C).

These findings were verified biochemically taking advantage of surface protein biotinylation. Receptors at the plasma membrane were labeled with a cleavable form of biotin (sulfo-NHS-

SS-biotin) and subjected to endocytosis. After cleavage of biotin from receptors remaining at the cell surface, the amount of internalized biotinylated MET was measured. Results confirmed that JNJ-605 severely affects MET endocytosis (Fig. 2D). This was not due to a general impairment of endocytic pathways, as treatment with JNJ-605 did not prevent ligand-induced EGFR endocytosis (Supplementary Fig. S2A,B).

In *MET*-amplified cells, receptor constitutive activation is the consequence of spontaneous dimerization/trans phosphorylation due to increased local density of the kinase [(16) and reviewed in (2)]. We therefore tested whether MET dimerization could be a pre-requisite for receptor endocytosis. To this end, we took advantage of a decoy MET receptor that encompasses the MET extracellular domain and binds to the full-length receptor, thus preventing MET homo dimerization and activation (17,18). In agreement with the ability of the decoy to reduce MET trans phosphorylation (17,18), we found that it severely affected both ligand-induced and constitutive MET endocytosis (Supplementary Fig. S3A,B).

We then assessed if MET kinase inhibition leads to receptor accumulation at the plasma membrane. A549 and the *MET*-amplified cell lines Hs746T and EBC-1 were treated with JNJ-605 for 2, 10 or 24 hours, and proteins exposed at the cell surface were labeled with non-cleavable biotin. Total MET was immuno-precipitated from the various conditions and the amount of labeled surface receptor was revealed by streptavidin. In agreement with our initial observation (Fig. 1A-F) and with the endocytosis data (Fig. 2A-D), treatment with JNJ-605 increased the amount of MET at the cell surface in all tested cell lines (Fig. 3A). This effect was not restricted to JNJ-605 but was exerted also by other MET kinase inhibitors such as PHA665752 and crizotinib (Fig. 3B).

Finally, we evaluated whether inhibition of MET kinase activity might alter recycling from endosomal compartments using a pulse-chase approach with sulfo-NHS-SS-biotin. The amount of biotinylated MET remaining within endosomal compartments after chasing for 15

11

or 30 minutes, in the presence or absence of JNJ-605, was assayed by capture-ELISA. While JNJ-605 inhibited MET endocytosis (Fig. 2A-D), it had no effect on the amount of its intracellular pool in any cell line tested (Fig. 3C). Thus, our results show that pharmacological kinase inhibition blocks MET endocytosis, but not recycling, causing accumulation of the receptor at the plasma membrane.

Removal of the MET inhibitor JNJ-605 causes rebound effects on kinase phosphorylation and cell proliferation

We initially analyzed re-phosphorylation of MET following inhibitor withdrawal in time course immunofluorescence experiments on H1993 cells treated with JNJ-605 overnight and then released from inhibition through a rapid washout procedure. We observed that the amount of phospho-MET increased rapidly after inhibitor washout becoming markedly higher, compared to control, 2 hours after the release, with a peak around 8 hours (Fig. 4A,B). This abrupt re-phosphorylation was transient as it went back to control levels between 48 and 72 hours following release (Fig. 4A,B). Following drug withdrawal, we detected a small fraction of phospho-MET on early endosomes (Fig. 4C). The extent of internalization of the active receptor was modest immediately after treatment discontinuation, and reached control levels along time (Fig. 4C) indicating that endocytosis resumed with slow kinetics. MET re-phosphorylation was confirmed by immunoblotting of lysates from H1993 and EBC-1 cells (Fig. 4D).

To explore the mechanisms underlying this prolonged and increased MET activation after drug removal, we investigated whether negative regulators of MET phosphorylation could be affected by MET blockade and subsequent release. Among the phosphatases known to act on MET, PTP1B plays a major role being responsible for dephosphorylation of tyrosines 1234 and 1235 within the MET catalytic domain (19). Autophosphorylation on these residues is

required for subsequent phosphorylation on other tyrosines in the MET docking site and for full MET activation (20,21). Importantly, loss of PTP1B is known to cause MET hyper-phosphorylation (19).

We found that PTP1B protein expression was reproducibly reduced, both in the EBC-1 and H1993 cell lines, upon JNJ-605 treatment; this down-modulation was maintained after inhibitor washout, inversely correlating with the increased MET phosphorylation (Fig. 4D). Although the molecular underpinnings of PTP1B modulation remain to be determined, these findings point to down-regulation of PTP1B as a potential mechanism to promote rebound MET hyper-phosphorylation after drug removal.

To investigate the effects of increased receptor activity we looked at ERK1/2 and AKT as these are the two major MET-dependent pathways that sustain growing and survival in the MET-amplified cells (6). Multiplex quantitative assessment confirmed that release from JNJ-605 increased ERK1/2 re-phosphorylation of about 2-fold both in EBC-1 and H1993 cells (Fig. 5A). The increase measured on AKT was of about 1.5-fold in both cell lines (Fig. 5A).

Finally, we investigated whether the observed rebound phosphorylation and activation of MET signaling pathways was accompanied by re-entering of cells into the cycle. We found that, in H1993 and EBC-1 cell lines, the number of cells in S phase 24 hours after inhibitor washout was nearly doubled compared to controls (Fig. 5B).

Based on the extensive crosstalk between MET and other RTKs, we investigated whether rebound activation would also involve other receptors. Stimulation with EGF, NRG1-β1 or PDGF did not increase the S-phase entry of cells following inhibitor withdrawal (Supplementary Figure S4A). Moreover, phosphorylation of EGFR and HER3 was not significantly enhanced by JNJ-605 washout (Supplementary Figure S4 B,C). Thus, massive entry of cells into S-phase following inhibitor withdrawal appears to depend primarily on MET activation.

In conclusion, removal of an ATP-competitive, reversible, MET inhibitor restores MET phosphorylation and signaling, re-programming cells for proliferation.

Treatment with a MET therapeutic antibody abrogates rebound MET activation *in vitro*

We tested whether the rebound effect, generated by kinase inhibition removal, could be prevented by a complementary pharmacological treatment, such as the therapeutic monovalent DN30 (MvDN30). This antibody down regulates the receptor by stimulating the activity of proteases at the cell surface (22). MvDN30 has no agonistic effect on MET (11), including the ability to trigger endocytosis (shown in Supplementary Fig. S1, shedding activity is shown in Supplementary Fig. S5).

We found that, when MvDN30 was added to EBC-1 cells immediately after inhibitor washout and kept for 24 hours, it led to almost complete abrogation of ERK1/2 and AKT phosphorylation, consistent with the down-regulation of the MET protein (Fig. 6A). In agreement, addition of MvDN30 after JNJ-605 removal severely dampened re-entry of cancer cells into the cycle (Fig. 6B) preventing the rebound effects caused by kinase inhibitor washout.

In a complementary approach, we tested whether removal of MvDN30 from cells that were pre-treated exclusively with the antibody could result in rebound effects. Differently from JNJ-605, removal of MvDN30 did not promote MET/ERK/AKT re-phosphorylation and, consistently, it did not enhance cell entry into S-phase (Fig. 6C, D).

Discontinuation of the MET kinase inhibitor restores tumor cell proliferation and is counteracted by MvDN30 treatment *in vivo*

Based on the results obtained *in vitro*, we investigated whether JNJ-605 withdrawal might cause rebound MET activation and cancer cell growth *in vivo*. We initially evaluated the occurrence of rebound S-phase entry in experimental tumors established by injecting EBC-1 cells subcutaneously into NOD-SCID mice. When tumor size reached approximately 90 mm^3, mice were randomized and subjected to oral administration of JNJ-605 for five days. A control group of animals (CTR) did not receive the drug (Supplementary Fig. S6A). We measured the percentage of cells that entered the S phase of the cycle by injecting EdU, a thymidine analogue that is incorporated in the DNA of duplicating cells, 24 hours before harvesting the tumors. In the tumors in which treatment with JNJ-605 was interrupted for 3 and 5 days the number of proliferating cells was markedly higher compared to untreated tumors and it was accompanied by increased MET phosphorylation and ERK activation (Supplementary Fig. S6B,C). These findings show that discontinuation of the anti-MET kinase inhibitor favors marked and rapid resumption of tumor proliferative activity by rebound reactivation of the MET receptor and its downstream signaling cascade.

Next we investigated the ability of MvDN30 to counteract the rebound effect. To this end, we repeated the experiment. Two groups of animals were treated with JNJ-605 for five days; then, treatment was discontinued. One group was left untreated, while the other was intraperitoneally administered with MvDN30-PEG, the chemically stabilized form of MvDN30, suitable for *in vivo* application (12). After 7 days all animals, including the controls, were sacrificed (Fig. 7A). The burst of S-phase cells and the increase of MET/ERK activation induced upon JNJ-605 withdrawal were abrogated in the tumors that received MvDN30-PEG (Fig. 7B-D). Analysis of tumor volumes revealed that, after a short period of latency (three days), therapy dismissal resulted in tumor regrowth (Fig. 7E). Treatment with MvDN30-PEG, after JNJ-605 withdrawal, partly impaired this tendency (Fig. 7E). These

findings show that the resumption of tumor proliferative activity occurring upon discontinuation of the anti-MET kinase inhibitor is dampened by MvDN30-PEG treatment.

DISCUSSION

In clinical settings, discontinuation of tyrosine kinase inhibitors such as erlotinib and crizotinib has been found associated with a significant risk of rebound cancer growth or accelerated disease progression ("disease-flare") (23,24). Targeted therapy is usually discontinued when, after initial response, patients demonstrate disease progression, indicative that they have acquired resistance to the drug. However, because of the reported "flare", it has been recently recommended to minimize the washout period in this patient population before starting with a second line therapy or to continue it concurrently with the new treatment (25). Here, we provide evidence that release of MET blockade after treatment with a MET small-molecule inhibitor leads to rebound MET activation and cell proliferation both *in vitr*o and in experimental tumors *in vivo*.

Treatment with MET inhibitors blocks MET endocytosis, increasing the number of receptors at the plasma membrane. Rise in receptor concentration at the cell surface has been shown to promote trans phosphorylation, likely by favoring receptor dimerization (2,16). Accordingly, interfering with receptor dimerization through a decoy receptor inhibits MET trans phosphorylation and endocytosis [(17,18) and this study], supporting the role of increased receptor clustering in the rapid re-phosphorylation of MET after inhibitor washout. This initial re-phosphorylation is then enhanced and prolonged likely by the reduced expression of a critical MET-negative regulator, the phosphatase PTP1B (19). Loss of PTP1B not only increases MET phosphorylation and signaling, but it also dampens receptor trafficking to the early endosomal compartment (19,26), thus, the observed reduction in PTP1B levels could also account for the delayed kinetics of receptor endocytosis following inhibitor withdrawal. Even if the active receptor is primarily present at the cell surface during drug washout, a small fraction of phospho-MET can be detected on early endosomes. As early endosomes represent a relevant platform for activation of MET downstream pathways [(27-29) and

reviewed in (30)], endosomal MET signaling likely participates to the rebound effect.

The increased MET activation and cell entry into the S phase that we observed *in vitro* are reproduced also *in vivo* after treatment discontinuation. Even if the rebound effect is transient, it appears to be sufficient to resume tumor growth, with potential implications in the emergence of genetically fitter subclones or in the expansion of cancer stem cell subpopulations.

Among the strategies to target MET in cancer, antibodies have been generated including the monovalent MvDN30 (5) whose therapeutic efficacy has been shown so far only on experimental tumor models (11,12). Of note, treatment of cancer cells resistant to MET kinase inhibitors with the MvDN30 antibody severely reduces their viability (31). This re-sensitization of resistant cells to MET inhibition relies on the ability of MvDN30 to function synergistically with MET kinase inhibitors (31), as it exploits a different mechanism of action whereby the antibody induces protease-mediated receptor shedding from the cell surface. Based on this evidence, it has been proposed that discontinuous, combined treatment by MvDN30 and chemical inhibitors may increase the clinical response bypassing resistance to anti-MET target therapies (31). The evidence that MET blockade by kinase inhibition led to MET accumulation at the cell membrane as well as rebound phosphorylation and cell-cycle entry after inhibitor washout, with delayed endocytosis, provide the rational to test MvDN30 as a means to curb the rebound effect by removing MET from the cell surface. Our findings that, indeed, treatment with MvDN30 abolished the rebound effect further support the rationale of combined or alternate anti-MET therapies.

ACKNOWLEDGMENTS

REFERENCES

1.   Sawyers C. Targeted cancer therapy. Nature 2004;432(7015):294-7.
2.   Trusolino L, Comoglio PM. Scatter-factor and semaphorin receptors: cell signalling for invasive growth. Nat Rev Cancer 2002;2(4):289-300.
3.   Gherardi E, Birchmeier W, Birchmeier C, Vande Woude G. Targeting MET in cancer: rationale and progress. Nat Rev Cancer 2012;12(2):89-103.
4.   Danilkovitch-Miagkova A, Zbar B. Dysregulation of Met receptor tyrosine kinase activity in invasive tumors. J Clin Invest 2002;109(7):863-7.
5.   Comoglio PM, Giordano S, Trusolino L. Drug development of MET inhibitors: targeting oncogene addiction and expedience. Nat Rev Drug Discov 2008;7(6):504-16.
6.   Bertotti A, Burbridge MF, Gastaldi S, Galimi F, Torti D, Medico E, et al. Only a subset of Met-activated pathways are required to sustain oncogene addiction. Sci Signal 2009;2(102):er11.
7.   Serio G, Margaria V, Jensen S, Oldani A, Bartek J, Bussolino F, et al. Small GTPase Rab5 participates in chromosome congression and regulates localization of the centromere-associated protein CENP-F to kinetochores. Proc Natl Acad Sci U S A 2011;108(42):17337-42.
8.   Roberts M, Barry S, Woods A, van der Sluijs P, Norman J. PDGF-regulated rab4-dependent recycling of alphavbeta3 integrin from early endosomes is necessary for cell adhesion and spreading. Curr Biol 2001;11(18):1392-402.
9.   Palamidessi A, Frittoli E, Ducano N, Offenhauser N, Sigismund S, Kajiho H, et al. The GTPase-activating protein RN-tre controls focal adhesion turnover and cell migration. Curr Biol 2013;23(23):2355-64.
10.   Fu L, Medico E. FLAME, a novel fuzzy clustering method for the analysis of DNA microarray data. BMC Bioinformatics 2007;8:3.
11.   Pacchiana G, Chiriaco C, Stella MC, Petronzelli F, De Santis R, Galluzzo M, et al. Monovalency unleashes the full therapeutic potential of the DN-30 anti-Met antibody. J Biol Chem 2010;285(46):36149-57.
12.   Vigna E, Chiriaco C, Cignetto S, Fontani L, Basilico C, Petronzelli F, et al. Inhibition of ligand-independent constitutive activation of the Met oncogenic receptor by the engineered chemically-modified antibody DN30. Mol Oncol 2015;9(9):1760-72.
13.   Lutterbach B, Zeng Q, Davis LJ, Hatch H, Hang G, Kohl NE, et al. Lung cancer cell lines harboring MET gene amplification are dependent on Met for growth and survival. Cancer Res 2007;67(5):2081-8.
14.   Prat M, Crepaldi T, Pennacchietti S, Bussolino F, Comoglio PM. Agonistic monoclonal antibodies against the Met receptor dissect the biological responses to HGF. J Cell Sci 1998;111 (Pt 2):237-47.
15.   Smolen GA, Sordella R, Muir B, Mohapatra G, Barmettler A, Archibald H, et al. Amplification of MET may identify a subset of cancers with extreme sensitivity to the selective tyrosine kinase inhibitor PHA-665752. Proc Natl Acad Sci U S A 2006;103(7):2316-21.
16.   Ferracini R, Longati P, Naldini L, Vigna E, Comoglio PM. Identification of the major autophosphorylation site of the Met/hepatocyte growth factor receptor tyrosine kinase. J Biol Chem 1991;266(29):19558-64.

17.   Michieli P, Mazzone M, Basilico C, Cavassa S, Sottile A, Naldini L, et al. Targeting the tumor and its microenvironment by a dual-function decoy Met receptor. Cancer Cell 2004;6(1):61-73.

18.   Kong-Beltran M, Stamos J, Wickramasinghe D. The Sema domain of Met is necessary for receptor dimerization and activation. Cancer Cell 2004;6(1):75-84.

19.   Sangwan V, Paliouras GN, Abella JV, Dubé N, Monast A, Tremblay ML, et al. Regulation of the Met receptor-tyrosine kinase by the protein-tyrosine phosphatase 1B and T-cell phosphatase. J Biol Chem 2008;283(49):34374-83.

20.   Longati P, Bardelli A, Ponzetto C, Naldini L, Comoglio PM. Tyrosines1234-1235 are critical for activation of the tyrosine kinase encoded by the MET proto-oncogene (HGF receptor). Oncogene 1994;9(1):49-57.

21.   Rodrigues GA, Park M. Autophosphorylation modulates the kinase activity and oncogenic potential of the Met receptor tyrosine kinase. Oncogene 1994;9(7):2019-27.

22.   Petrelli A, Circosta P, Granziero L, Mazzone M, Pisacane A, Fenoglio S, et al. Ab-induced ectodomain shedding mediates hepatocyte growth factor receptor down-regulation and hampers biological activity. Proc Natl Acad Sci U S A 2006;103(13):5090-5.

23.   Chaft JE, Oxnard GR, Sima CS, Kris MG, Miller VA, Riely GJ. Disease flare after tyrosine kinase inhibitor discontinuation in patients with EGFR-mutant lung cancer and acquired resistance to erlotinib or gefitinib: implications for clinical trial design. Clin Cancer Res 2011;17(19):6298-303.

24.   Kuriyama Y, Kim YH, Nagai H, Ozasa H, Sakamori Y, Mishima M. Disease flare after discontinuation of crizotinib in anaplastic lymphoma kinase-positive lung cancer. Case Rep Oncol 2013;6(2):430-3.

25.   West H, Oxnard GR, Doebele RC. Acquired resistance to targeted therapies in advanced non-small cell lung cancer: new strategies and new agents. Am Soc Clin Oncol Educ Book 2013.

26.   Sangwan V, Abella J, Lai A, Bertos N, Stuible M, Tremblay ML, et al. Protein-tyrosine phosphatase 1B modulates early endosome fusion and trafficking of Met and epidermal growth factor receptors. J Biol Chem 2011;286(52):45000-13.

27.   Joffre C, Barrow R, Ménard L, Calleja V, Hart IR, Kermorgant S. A direct role for Met endocytosis in tumorigenesis. Nat Cell Biol 2011;13(7):827-37.

28.   Parachoniak CA, Luo Y, Abella JV, Keen JH, Park M. GGA3 functions as a switch to promote Met receptor recycling, essential for sustained ERK and cell migration. Dev Cell 2011;20(6):751-63.

29.   Muharram G, Sahgal P, Korpela T, De Franceschi N, Kaukonen R, Clark K, et al. Tensin-4-dependent MET stabilization is essential for survival and proliferation in carcinoma cells. Dev Cell 2014;29(4):421-36.

30.   Barrow-McGee R, Kermorgant S. Met endosomal signalling: in the right place, at the right time. Int J Biochem Cell Biol 2014;49:69-74.

31.   Martin V, Corso S, Comoglio PM, Giordano S. Increase of MET gene copy number confers resistance to a monovalent MET antibody and establishes drug dependence. Mol Oncol 2014.

FIGURE LEGENDS

Figure 1. Effects of kinase inhibition on MET localization.

Confocal images of H1993 (A) and Hs746T cells (D) mock treated or treated with 300nM JNJ-605 (indicated on top) for 2 hours at 37°C. Merged images show MET (green), EEA1 (red) and DAPI (blue). Portions of the endosomal compartment are boxed in the images and magnified in the insets below. Arrows point to the plasma membrane. Bar, otherwise specified, is 10 µm. B) and E) Bar graphs showing the percentage of MET that co-localizes with EEA1 in H1993 (B) and Hs746T (E) cells (means ± s.e.m; n=8). C) and F) Immunoblotting of total cellular lysates from H1993 (C) and Hs746T (F) cells.

Figure 2. Kinase inhibition blocks MET endocytosis.

A) MET endocytosis was assayed in A549, H1993 and Hs746T cell lines untreated (CTR) or treated for 15 min with HGF, or anti-MET antibody DO24, or control antibody (Ab unr.) in absence (mock) or presence of 300nM JNJ-605 (JNJ-605). Merged images show MET (green), EEA1 (red) and DAPI (blue). Magnifications show part of the endosomal compartment. B) MET endocytosis assays in presence of JNJ-605. C) Quantification of the percentage of MET that co-localizes with EEA1. Black bars, untreated cells, red bars cells treated with JNJ-605. Means ± s.e.m, n=8. CTR vs HGF- or DO24-treated cells $\#p < 0.0001$. Untreated vs JNJ-605-treated cells $**p < 0.005$. D) Biochemical endocytosis assays. Bar graphs represent the amount of internalized biotinylated MET in the cell lines indicated on top in untreated cells (black bars) or in cells subjected to JNJ-605 inhibition (red bars). Data are expressed as the percentage of internalised receptor, relative to the total amount of cell surface–labeled receptor. Values are the mean of three independent experiments ± SD performed in triplicate. $*** p < 0.0005$.

Figure 3. Inhibition of MET kinase causes receptor accumulation at the plasma membrane.

A) A549, Hs746T and EBC-1 cells were treated with JNJ-605 500nM for 2, 10 or 24 hours at 37°C, surface receptors were biotinylated and MET was immunoprecipitated (IP). Total lysates were run in input lanes (20 µg A549, 3 µg Hs746T and EBC-1). Streptavidin (strept.) reveals the amount of MET that accumulates at the plasma membrane. Immunoblotting was as indicated on the left. B) Hs746T cells were treated with different MET inhibitors (500nM) JNJ-605, PHA and crizotinib (CRIZ.) for 2 hours or over night and processed as in A). Immunoblotting was as indicated on the left. Total lysates were run in input lanes. C) MET recycling in the A549, Hs746T and EBC-1 cell lines. The amount of biotinylated MET remaining after chasing cells for 15 or 30 min in presence or absence of JNJ-605 was determined by capture-ELISA. The percentage of MET recycled to the plasma membrane is expressed as the difference between the amount of MET initially labeled at the cell surface and the intracellular biotinylated pool remaining after chasing [as in (8)]. Values are the mean of two independent experiments ± SD, each point done in triplicate. *P* values not significative.

Figure 4. Inhibitor washout promotes rebound MET activation.

A) H1993 cells were treated overnight with 500nM JNJ-605 and fixed (JNJ-605), or released from the inhibition and fixed at the time points indicated on top. Controls (CTR) are untreated cells. Confocal merged images show total MET (green), phospho-MET (red), EEA1 (magenta) and DAPI (blue). B) Bar graph reporting the ratio of pixel intensity between phospho- and total MET (means ± s.e.m, n=8). C) Bar graph showing the percentage of phospho-MET that colocalizes with EEA1 (means ± s.e.m, n=8). D) Total cellular lysates from H1993 and EBC-1 cells treated as in A) were run on two different gels. We

immunoblotted one gel (run with 40 µg of lysates) with anti-phospho-MET and anti-MET (total) antibodies, the second gel (run with 10 µg of lysates) with anti-PTP1B and anti-β-tubulin. Heat maps below the western blots represent the amount of PTP1B levels normalized on β-tubulin measured by densitometry. Mean values from two independent experiments.

Figure 5. Inhibitor washout promotes rebound MET signaling.

A) Heat map of phosphoproteins response to inhibitor withdrawal obtained by MesoScale analysis. The color scale bar represents relative protein phosphorylation changes calculated as $\log_2$ of the mean of two independent experiments done in duplicates. Phospho-ERK $p< 0.03$; phospho-AKT $p< 0.007$. B) Bar graphs showing the percentage of S-phase H1993 and EBC-1 cells treated with JNJ-605 and released for the time indicated on bottom. Values are the mean of three independent experiments ± s.e.m.

Figure 6. Rebound effects caused by inhibitor removal are prevented by MvDN30 treatment.

A) Immunoblotting of total cellular lysates from EBC-1 cells treated over night with 500nM JNJ-605, released from inhibition, and lysed at different time points (4h, 8h, 24h and 48h after washout). CTR, untreated cells; JNJ-605, cells that were not released; 24h+MvDN30, cells that were released from JNJ-605 and kept in presence of the MvDN30 antibody for 24 hours; 24h+Fab unr., cells that were released in presence of an unrelated Fab antibody for 24 hours. B) Bar graphs showing the percentage of S-phase EBC-1 cells treated as in (A). Values are the mean of three independent experiments ± s.e.m. C) EBC-1 and Hs746T cells were mock treated (CTR) or treated with MvDN30 [57.4 µg/ml] (MvDN30) overnight. Cells were released from the treatment through a washout procedure identical to the one used for JNJ-605 (24h MvDN30 washout) and lysed 24 hours later. Total cell lysates were blotted as

indicated on the left. Detection of AKT and ERK was done on different gels (with phospho and total proteins on the same gel). D) Bar graph showing the % of EBC-1 cells in S-phase in the samples indicated below (means ± SD, n = 4).

Figure 7. Rebound effects are prevented by MvDN30 *in vivo*.

A) Experimental design. B) Bar graph showing the % of EdU-positive area normalized for DAPI staining (means ± s.e.m,; 8 fields/tumor were quantified). C) Representative merged confocal images of tumor sections showing the nuclei in blue and the EdU-positive cells in red. Bar is 50 μm. D) Representative images from tumor sections analyzed by immunohistochemistry with anti phospho-MET (top panel) and anti phospho-ERK (bottom panel) antibodies. In the phospho-MET panel, magnifications are also shown in the insets. Bar is 50 μm. E) Curves (means ± s.e.m.) refer to tumor volumes normalized on day 23 in mice treated as indicated in the legend.

A H1993
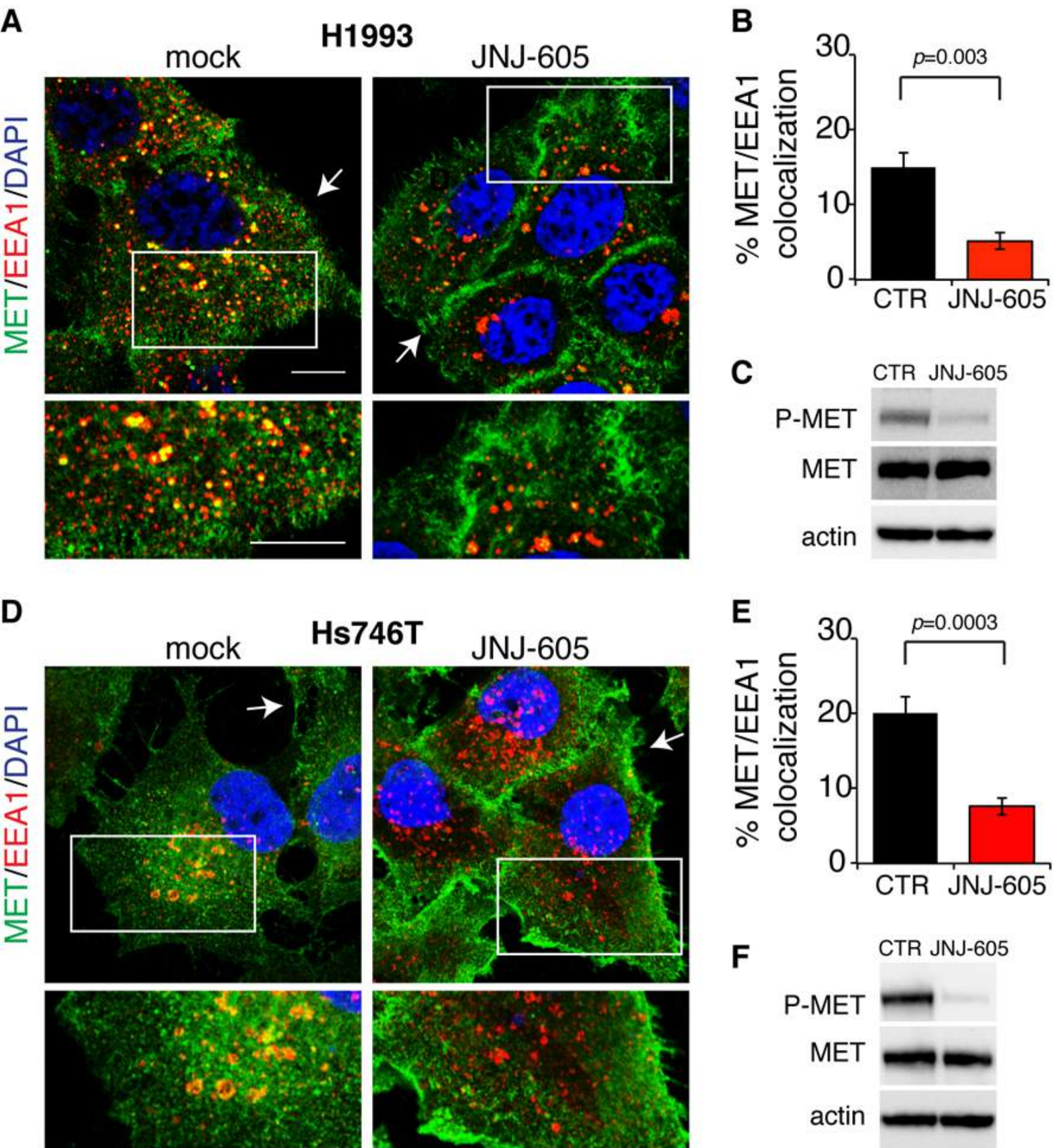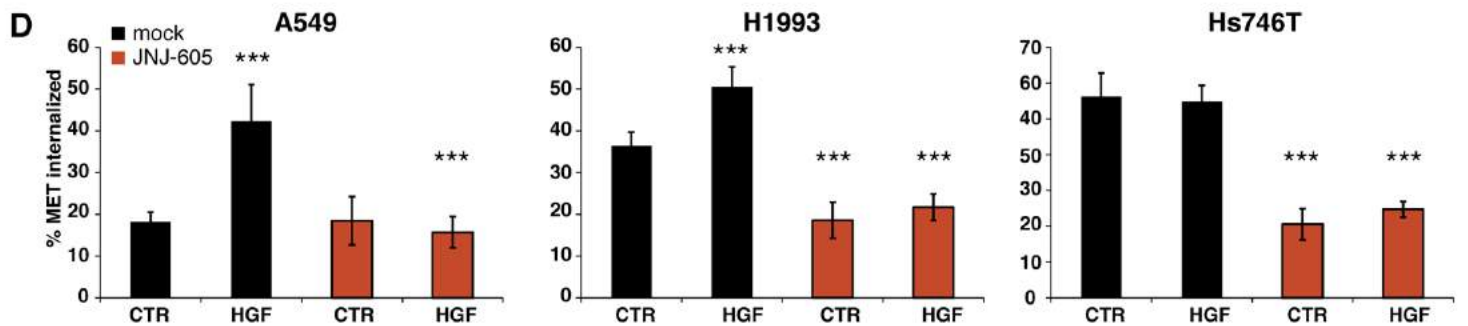
mock   JNJ-605

MET/EEA1/DAPI

B

% MET/EEA1 colocalization

p=0.003

CTR   JNJ-605

C

CTR   JNJ-605

P-MET

MET

actin

D Hs746T

mock   JNJ-605

MET/EEA1/DAPI

E

% MET/EEA1 colocalization
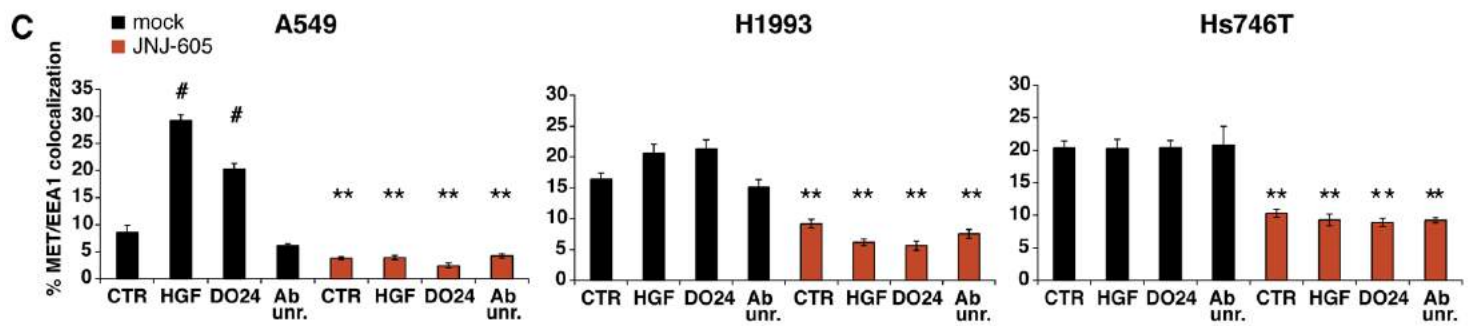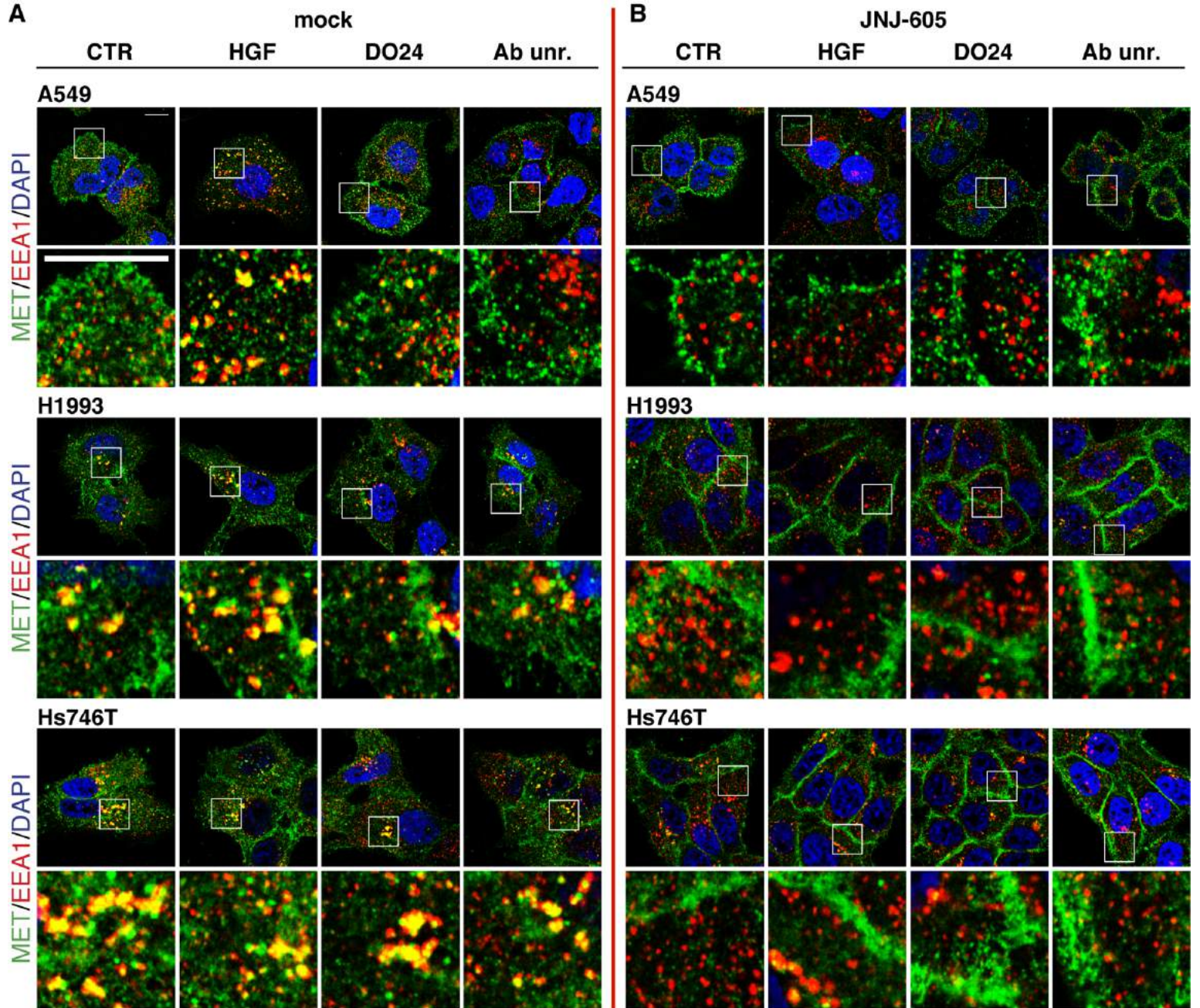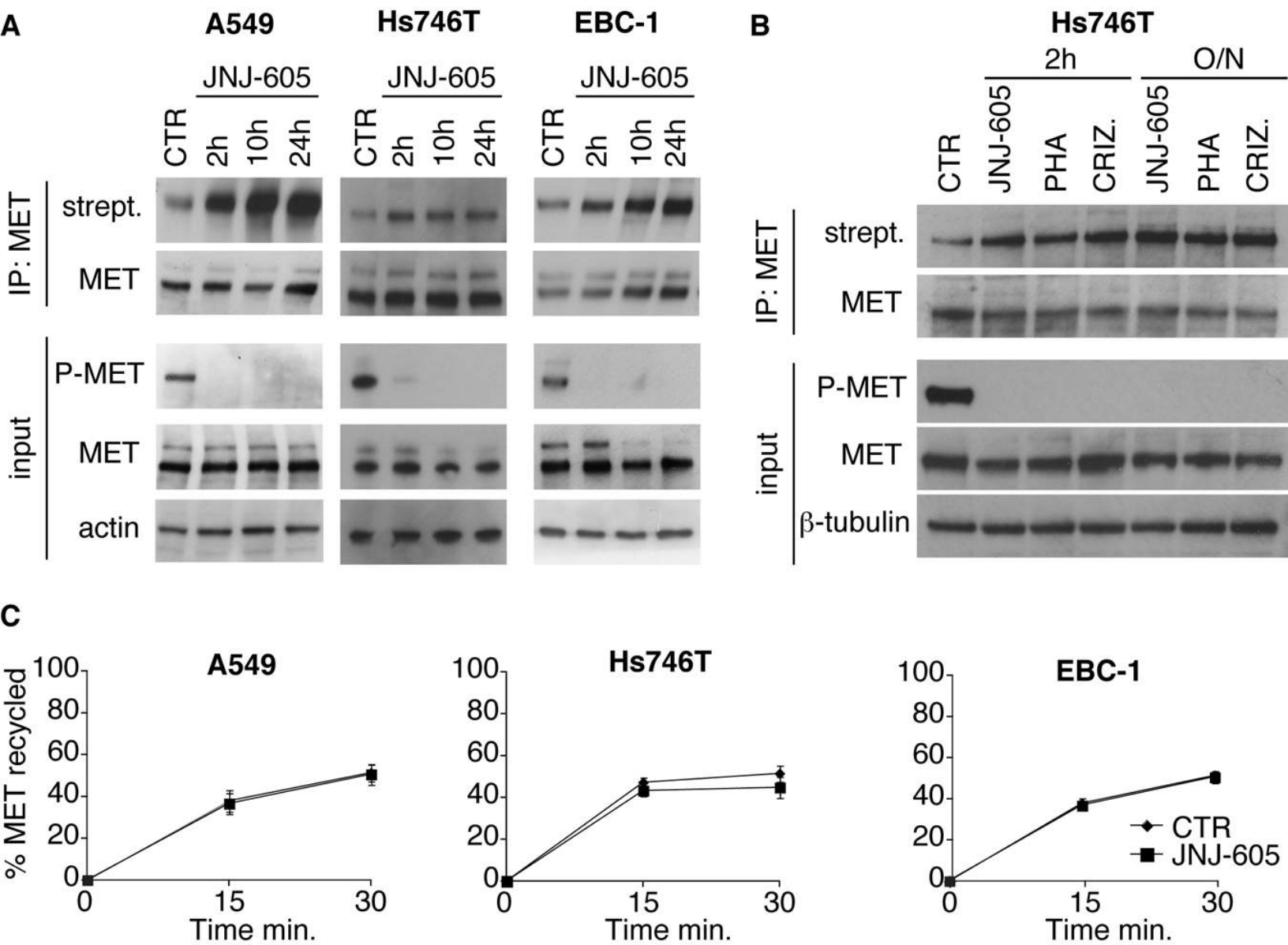
p=0.0003

CTR   JNJ-605

F

CTR   JNJ-605

P-MET

MET

actin

Figure 1

Figure 2

Figure 3

Figure 4

A

ERK

CTR JNJ 2h 24h

H1993
EBC-1

AKT

CTR JNJ 2h 24h

H1993
EBC-1

-1.0   +1.0
log $_2$R

B

H1993

S phase cells (%)

p=0.02

CTR   JNJ-605   4h   8h   24h   48h

JNJ-605 washout

EBC-1

p=0.005

CTR   JNJ-605   4h   8h   24h   48h

JNJ-605 washout

Figure 5

Figure 6

A

Days

Cell injection

JNJ-605 treatment

JNJ-605 withdrawal → MvDN30 treatment

Control

w/o JNJ-605

w/o JNJ w MvDN30

B

p=0.0001   p=0.0001

EdU-positive area/DAPI (%)

CTR   w/o JNJ   w/o JNJ w MvDN30

C

JNJ-605 withdrawal

CTR   w/o JNJ-605   w/o JNJ-605 w MvDN30

D

CTR   w/o JNJ-605   w/o JNJ-605 w MvDN30

P-MET

P-ERK

E

CTR
JNJ-605 withdrawal
JNJ-605 withdrawal w MvDN30

Tumor volume fold change (normalized on day 23)

Days

Figure 7